



**HAL**  
open science

## Modelling of the sulfuric acid attack on different types of cementitious materials

Anaïs Grandclerc, Patrick Dangla, Marielle Gueguen Minerbe, Thierry  
Chaussadent

► **To cite this version:**

Anaïs Grandclerc, Patrick Dangla, Marielle Gueguen Minerbe, Thierry Chaussadent. Modelling of the sulfuric acid attack on different types of cementitious materials. *Cement and Concrete Research*, 2018, 105, 67 p. 10.1016/j.cemconres.2018.01.014 . hal-01880755

**HAL Id: hal-01880755**

**<https://hal.science/hal-01880755v1>**

Submitted on 25 Sep 2018

**HAL** is a multi-disciplinary open access archive for the deposit and dissemination of scientific research documents, whether they are published or not. The documents may come from teaching and research institutions in France or abroad, or from public or private research centers.

L'archive ouverte pluridisciplinaire **HAL**, est destinée au dépôt et à la diffusion de documents scientifiques de niveau recherche, publiés ou non, émanant des établissements d'enseignement et de recherche français ou étrangers, des laboratoires publics ou privés.

## **Modelling of the sulfuric acid attack on different types of cementitious materials**

GRANDCLERC Anaïs <sup>a\*</sup>, DANGLA Patrick <sup>b</sup>, GUEGUEN-MINERBE Marielle <sup>a</sup> and  
CHAUSSADENT Thierry <sup>a</sup>

<sup>a</sup> Université Paris-Est, MAST, CPDM, IFSTTAR, F- 77447 Marne-la-Vallée, France

<sup>b</sup> Université Paris-Est, Laboratoire Navier (UMR 8205), CNRS, École des Ponts ParisTech,  
F-77455 Marne-La-Vallée, France

\*anais.grandclerc@ifsttar.fr

### **Abstract**

A chemical-reactive transport model was used to simulate the sulfuric acid attack of cement pastes based on ordinary Portland cement (CEM I), blended Portland cements (CEM III, CEM IV, and CEM V), and calcium aluminate cement (CAC). This model accounts for the dissolution of cement hydrates (portlandite, C-S-H, hydrogarnet), and the precipitation of deterioration products (ettringite and gypsum). Moreover, diffusion of the aqueous species in the pore space in the material is considered. With this model, we can get the hydrate contents, the porosity, and the deterioration phase contents throughout a sulfuric acid attack. Two indicators are defined to predict the service life of the cementitious materials: the deterioration depth and the dissolved calcium content. These two indicators showed that calcium aluminate cement provide a better resistance to sulfuric acid attack than that of Portland cements. This better resistance is mainly due to the partial dissolution of CAC hydrate as opposed to the total dissolutions of CH and C-S-H.

**Keywords: Deterioration (C.), Calcium Aluminate Cement (D.), Portland cement (D.), Modelling (E.), Acid attack**

### **1. Introduction**

Concrete can undergo severe deteriorations in sewer pipe conditions, caused by gaseous hydrogen sulphide (Figure 1) [1, 2]. Concrete gravity sewers are divided into two parts: a liquid part and an aerial part (sewer atmosphere). The liquid part contains waste water which is composed of sulfate ions and sulfate reducing bacteria (SRB). The cementitious wall in the aerial part is covered by a biofilm mainly

28 composed of sulphur-oxidizing bacteria (SOB). Aqueous hydrogen sulfide is produced in the anaerobic  
29 zone (waste water stagnation) from the reduction reaction of sulfate ions due to sulfate reducing bacteria.  
30 Then, H<sub>2</sub>S escapes into the sewer atmosphere, where it is adsorbed onto the cementitious wall [3]. Due  
31 to the high relative humidity at the surface of the wall, gaseous hydrogen sulphide dissociates into  
32 hydrogen ions and sulfide ions. Hydrogen ions contribute to surface pH neutralization, giving rise to the  
33 biofilm development [4]. Under such aerobic conditions, sulfide ions oxidize into several sulphur  
34 species, which are used as nutrients for the microorganisms of the biofilm. Sulfuric acid is produced by  
35 the oxidation reactions of these sulphur species [5, 6]. This acid attacks the cementitious walls and  
36 produces gypsum and ettringite [7, 8], which are expansive and cause severe damage of the sewer  
37 system. The sulfuric acid produced by these microorganisms diffuses through the altered layer and  
38 continually attacks the underlying concrete [9].

39 Numerical models of acid attack of cementitious materials [10-17] can be found in the literature. One  
40 of these models simulating the biochemical process and the sulfide oxidation is named “Wastewater  
41 Aerobic/anaerobic Transformations in Sewer” (WATS) [10, 11]. Another study [12] simulates sulfuric  
42 acid attack with a diffusion-reaction based model with a moving boundary to predict the corrosion rate.  
43 A reactive-transport model (HYTEC [13]; [14]) was also used to simulate the attack of cementitious  
44 materials by different types of organic acids. This model takes into account chemical interactions  
45 between these different organic acids and hydrates of cementitious materials based on Portland cement.  
46 Another model [15] has been proposed to simulate the acid attack of OPC and is based on the HYTEC  
47 model [14]. In this model, the dissolution of the main hydrates of the cementitious materials and the  
48 precipitation of deterioration products are simulated, using chemical equilibrium associated with  
49 thermodynamic constants and the transport of different species during sulfuric acid attack.

50 Some experimental studies [9, 18-21] in the literature have focused only on sulfuric acid attack of  
51 cementitious materials. For cementitious materials based on Portland cement, Bassuoni et al. [18]  
52 observed the dissolution of portlandite and the decalcification of C-S-H, which are the main hydrates of  
53 Portland cement, leading to mass loss. Kawai et al. [19] showed that cementitious materials containing

54 a high amount of silica fume have a better resistance than those containing fly ash or blast furnace slag.  
55 Jiang et al. [21] determined deterioration product localizations during these chemical reactions. Gypsum  
56 is the first product formed from the reaction between hydrates and sulfuric acid followed by ettringite  
57 localized near the undeteriorated concrete. Thermodynamically, ettringite is stable at pH greater than  
58 10.7 [22] and forms only for high pH conditions. All these tests were performed on cementitious  
59 materials based on Portland cement or blended Portland cements. Several *in-situ* experiments (with  
60 microorganism presence) carried out by Alexander and Fourie [8] and Herisson et al. [23] suggested  
61 that cementitious materials based on calcium aluminate cement (CAC) have a better resistance than that  
62 of ordinary or blended Portland cements. Moreover, several laboratory tests of biodeterioration also  
63 showed better resistance for CAC materials [24-27].

64  
65 In the present research, the behavior of cementitious materials based on different types of cement in  
66 contact with sulfuric acid was simulated with a predictive model based on the model of Yuan et al. [15].  
67 The cements were ordinary Portland cement (CEM I), blended Portland cements (CEM III, CEM IV,  
68 and CEM V), and calcium aluminate cement (CAC). The aim of this study was to predict deterioration  
69 depth of cement subjected to sulfuric acid attack and to determine which one has a better resistance to  
70 this kind of corrosion. In this study, the biological acid production, depending on numerous parameters,  
71 is not modeled. Instead, it is assumed that, due to a lack of data concerning interaction of microorganisms  
72 and cementitious materials and its consequence on acid production, the considered hypothesis is that  
73 microorganisms produce sulfuric acid in such a way that sulfuric acid concentration is constant. This  
74 model is then static. Despite of this hypothesis, the model results obtained may be compared with those  
75 from experimental *in-situ* and laboratory tests for which microorganism activity can be dependent on  
76 environmental and material parameters.

77

## 78 **2. Hydrate composition of cements**

79 The cementitious materials considered were cement pastes with a water to cement ratio of 0.4. The  
80 hydrate compositions and contents are presented in Table 1 and expressed in mole per liter of cement

81 paste. Initial data used for the model are porosity and hydrate amounts for each type of cement. For  
82 cement pastes based on CEM I, CEM III, CEM IV, and CEM V cements, the main hydrates are calcium  
83 silicate hydrate (C-S-H) and portlandite (CH) and for cement pastes based on calcium aluminate cement,  
84 the main hydrates are hydrogarnet ( $C_3AH_6$ ) and gibbsite ( $AH_3$ ). The chosen porosities are those of  
85 mortars, even if in the model, the cementitious materials considered are cement pastes. This  
86 consideration allows comparing model results (diffusion-controlled model leading to a high effect of the  
87 porosity) and experimental results.

88 Hydrate amounts were experimentally measured by TGA and Rietveld XRD techniques and the  
89 porosities were measured by the water absorption method [28]. The portlandite contents for CEM III,  
90 CEM IV, and CEM V cements are lower than that for CEM I cement, because the clinker is substituted  
91 by other compounds: blast furnace slag for CEM III cement, natural pozzolans for CEM IV cement, and  
92 a combination of blast furnace slag and fly ash for CEM V cement. In this model, the other phases of  
93 blended Portland cements (hydrates from the additions and anhydrous phases) were not taken into  
94 account in the chemical processes and the differences between the Portland cements are only controlled  
95 by the portlandite and C-S-H contents and the porosity.

96 With the purpose of comparing the behavior of cement pastes, the same calcium content is considered  
97 for all the cement, namely 6 mol/L. The C-S-H content is then deduced from a calcium to silicon ratio  
98 equal to 1.7 and the CH content. This assumption which may not reflect the reality, was considered with  
99 the aim of giving the same potential of calcium dissolution to all materials. Indeed, it is clear that the  
100 more the calcium content the better the resistance to calcium dissolution.

101 For the CAC materials, there are four main hydrates:  $C_3AH_6$ ,  $AH_3$ ,  $C_2AH_8$ , and  $CAH_{10}$ . If CAC paste  
102 undergoes heat treatment during the hydration mechanisms, the major hydrate is the stable hydrogarnet  
103 ( $C_3AH_6$ ) but if the hydration mechanisms take place at room temperature, the major hydrates formed are  
104 two metastable phases ( $CAH_{10}$  and  $C_2AH_8$ ).  $AH_3$  (gibbsite) is formed in both cases. During heat  
105 treatment, the conversion reaction provokes the transformation from metastable hydrate to the stable  
106 hydrate. The conversion reactions are partial and begin from a curing temperature of 28°C, reaching a

107 conversion rate of 100% for a temperature of 60°C [29]. For the model, only a CAC paste with  $C_3AH_6$   
108 as the main hydrate is considered. Lamberet et al. [30] indicate that the gibbsite ( $AH_3$ ) is stable for a  
109 surface pH of the cementitious material between 4 and 11. The CAC cement paste simulated in this  
110 study has a surface pH of 12 in the initial state. Therefore, gibbsite is not present initially. This hydrate  
111 can precipitate when the cementitious material is carbonated, inducing a surface pH around 7-8.  
112 However, the carbonation is not considered in this study and so the initial content is taken to zero (Table  
113 1).

### 114 **3. Modelling of the $H_2SO_4$ attack of concrete**

#### 115 **3.1. Chemical reactions and thermodynamic constants**

116 The reactive-transport model presented in Yuan et al. [15] takes into account the dissolution of CH and  
117 C-S-H and the precipitation of gypsum, so only the phase diagrams of the systems CaO-SiO<sub>2</sub>-H<sub>2</sub>O and  
118 CaO-SO<sub>3</sub>-H<sub>2</sub>O were considered. Alkali ions were also included in the system. In the present study, the  
119 model was improved by considering the system CaO-Al<sub>2</sub>O<sub>3</sub>-SO<sub>3</sub>-H<sub>2</sub>O, in addition to CaO-SiO<sub>2</sub>-H<sub>2</sub>O.

120 All the dissolution reactions implemented in the new model are listed in Table 2, for the heterogeneous  
121 reactions (in solid and aqueous phases) and in Table 3 for the homogeneous reactions (in only aqueous  
122 phase). The thermodynamic constant values are obtained from a data base (*CEM DATA 14.01*). This  
123 system contains stable and metastable phases. For CAC materials, Damidot et al. [31] determined that  
124 the metastable phase AFm crystallizes only when  $CAH_{10}$  and  $C_2AH_8$  are formed at 25°C, whereas the  
125 stable phase AFt (ettringite) crystallizes only when  $C_3AH_6$  is formed. As a result, in this system, AFm  
126 does not precipitate during the simulation.

#### 127 **3.2. Stability of solid phases**

128 The stability of each solid phase can be described by the equality between the equilibrium constant (K)  
129 and the ion activity product (Q). The ratio between Q and K defines the saturation index  $\beta$ . If  $\beta$  is lower  
130 than unity, the solid phase would not precipitate and if  $\beta$  is greater than unity, the solid phase would  
131 precipitate. For each solid phase, a saturation index is defined as a function of  $\beta_{CH}$ ,  $\beta_{AH_3}$ , and  $\beta_{H_2SO_4}$ ,

132 according to equations 1 to 6.  $\beta_{CH}$ ,  $\beta_{AH3}$ , and  $a_{H2SO4}$  are respectively the saturation indexes of portlandite  
133 and gibbsite and the activity of  $H_2SO_4$  (taken equal to  $H_2SO_4$  concentration) and they are considered as  
134 primary variables. After the Gibbs phase rule, the system  $CaO-SO_3-Al_2O_3-H_2O$  has 3 degrees of freedom  
135 at the most (at constant pressure and temperature), namely  $\beta_{CH}$ ,  $\beta_{AH3}$ , and  $a_{H2SO4}$ . The other saturation  
136 indexes can be derived from the mass action law under the form:

$$137 \quad \beta_{CSH2} = 10^{31.4} \beta_{CH} a_{H2SO4} \quad (1)$$

$$138 \quad \beta_{C3AH6} = 10^{4.59} \beta_{CH}^3 \beta_{AH3}^2 \quad (2)$$

$$139 \quad \beta_{CAH10} = 10^{-0.22} \beta_{CH} \beta_{AH3}^2 \quad (3)$$

$$140 \quad \beta_{C2AH8} = 10^{67.4} \beta_{CH}^2 \beta_{AH3}^2 \quad (4)$$

$$141 \quad \beta_{AFm} = 10^{38.4} a_{H2SO4} \beta_{CH}^4 \beta_{AH3}^2 \quad (5)$$

$$142 \quad \beta_{AFt} = 10^{107.5} \beta_{CH}^6 \beta_{AH3}^2 a_{H2SO4}^3 \quad (6)$$

143 From equations 1 to 6, the stability zones of each solid phase included in this system are plotted in the  
144 phase diagram (Figure 2).

145 The continuous decalcification of C-S-H, during acid attack, is simulated in the present study by a  
146 thermodynamic approach presented in [32].

### 147 **3.3. Kinetic law**

148 Portlandite,  $AH_3$ , and C-S-H are assumed in equilibrium with the solution. Dissolution and precipitation  
149 rates for  $C_3AH_6$ , gypsum, ettringite, and AFm are governed by a simple kinetic law (Equation 7).

$$150 \quad \frac{dn_A}{dt} = R_A (\beta_A - 1) \quad (7)$$

151 In Eq. (7),  $n_A$  is the amount of solid A in mol/L,  $R_A$  is the kinetic factor of the solid A in mol/L/s and  $\beta_A$   
152 is the saturation index of the solid A.

153 The kinetic factors introduced in this law ( $R_{C_3AH_6}$ ,  $R_{AFt}$ ,  $R_{AFm}$ , and  $R_{\text{gypsum}}$ ) are adjusted so that  
154 equilibrium is quickly reached. Indeed, this kinetic law is governed by interface reactions. But, interface  
155 reactions are quicker than diffusion of aqueous species in the porous system in cementitious materials.  
156 As a result, the kinetic factors should be fixed as high as possible value, so as to get a saturation index  
157 as close as possible to 1. But, the model does not converge with too big kinetic factors, so some  
158 simulation tests are performed by increasing the factors as high as possible. The values chosen are  
159 presented in Table 4.

### 160 3.4. Porosity change

161 During the chemical reactions, the change in porosity ( $\Delta\phi$ ) is given by the volume change of the solid  
162 phases ( $\Delta V_{\text{solid}}$ ) according to equations 8 and 9.

$$163 \Delta\phi = -\Delta V_{\text{solid}} \quad (8)$$

164 Where  $V_{\text{solid}} = \sum_i V_i n_i$  with summation over all solids,  $V_i$  is the molar volume of each solid phase of  
165 the cement paste in L/mol and  $n_i$  is the amount of each solid phase in mol/L (CH, C-S-H,  $C_3AH_6$ ,  $AH_3$ ,  
166  $C_2AH_8$ ,  $CAH_{10}$ ,  $C\bar{S}H_2$ , AFm, and AFt).

167 The molar volume of C-S-H ( $V_{C-S-H}$ ) included in equation 9 is a function of the calcium to silicon ratio,  
168 according to [15].

$$169 V_{C-S-H}(x) = (x/x_0)V_{C-S-H}^0 + (1 - x/x_0)V_{SH} \quad (9)$$

170 Where  $x$  is the calcium to silicon ratio at a fixed time of sulfuric acid attack,  $x_0$  is the initial calcium to  
171 silicon ratio of the cement paste ( $C/S = 1.7$ ),  $V_{C-S-H}^0$  and  $V_{SH}$  are the molar volumes of C-S-H at the  
172 initial state ( $78 \text{ cm}^3/\text{mol}$  for  $C_{1.7}SH_{2.1}$ ) and of silica gel ( $29 \text{ cm}^3/\text{mol}$ ).

### 173 3.5. Reactive transport model

174 The system is controlled by chemical equilibrium but also by the transport of aqueous species. The  
175 coupling between these two mechanisms is taken into account within the modelling platform Bil [33],

176 based on the finite volume method. This coupling is treated with a mass balance equation (Equation 10),  
177 a global balance equation for the charge (Equation 11), and an equation for the electroneutrality to form  
178 an electroneutral pore solution (Equation 12). These equations are detailed in the study of Yuan et al.  
179 [15].

$$180 \quad \partial n_A / \partial t = -\text{div } \mathbf{w}_A \quad (10)$$

$$181 \quad \text{div } \underline{i} = 0 \quad (11)$$

$$182 \quad \sum_i z_i \rho_i = 0 \quad (12)$$

183 Where  $\underline{i} = \sum_i z_i \mathbf{w}_i$  is the ionic current and  $n_A$  is the mole content of element A in all phases per unit  
184 volume,  $\mathbf{w}_A$  is the molar flow vector of element A in the liquid phase,  $z_i$  is the ionic valence of  $i$ ,  $\mathbf{w}_i$  is  
185 the molar flow of  $i$ , and  $\rho_i$  is the concentration of  $i$ .

186 The transport of aqueous species is governed by the Nernst-Planck equation, previously detailed in the  
187 study of Yuan et al. [15]. According to Bazant-Najjar law [34], the evolution of the effective diffusion  
188 coefficient is:

$$189 \quad D_p / D_0 = 2.9 \cdot 10^4 \cdot \exp(9.95 \cdot \phi) \quad (13)$$

190  $D_p$  is the effective diffusion coefficient of aqueous species in the porous materials,  $D_0$  is the effective  
191 diffusion coefficient in bulk water and  $\phi$  is the porosity of the system at the current time and defined by  
192 the equation 8.

### 193 **3.6. Description of the simulations**

194 These one dimensional (1D) studies aim at simulating the chemical processes in sewer pipes made of  
195 different cement types (CEM I, CEM III, CEM IV, CEM V cements, and CAC). The simulations are  
196 conducted in 1D only. The 2 cm long sample is discretized in 200 elements (finite volume). The  
197 boundary surface represents the interface between the cementitious materials and the  $\text{H}_2\text{SO}_4$  solution.  
198 The initial  $\text{H}_2\text{SO}_4$  concentration in the pore solution of samples is set to  $10^{-32}$  mol/L, a very small value

199 consistent with the stability of the cement hydrates. At the boundary surface, the  $\text{H}_2\text{SO}_4$  concentration  
200 is set to  $10^{-1}$  mol/L, in order to study the deteriorations in extreme conditions. The damage model caused  
201 by gypsum formation as modeled in [15] was not extended to CAC system because this is ettringite  
202 which is mainly formed in CAC. So, in order to compare the durability of cement pastes, the  
203 deterioration depth is introduced as the distance between the first point where the porosity exceeds the  
204 initial porosity and the boundary surface.

## 205 **4. Results and Discussion**

### 206 **4.1. Profiles of the solid content**

207 The initial data for each type of cementitious material are summarized in Tables 1 and 4. All the results  
208 are simulated for one year with a  $\text{H}_2\text{SO}_4$  concentration of  $10^{-1}$  mol/L at the boundary surface of the  
209 cement pastes. The calculated profiles of solid phase contents, of the calcium to silicon ratio for the  
210 Portland cements and of the porosity, are plotted in Figure 3.

#### 211 **4.1.1. Profiles of the solid contents for ordinary or blended Portland cements**

212 As indicated in Figure 3, the initial amount of portlandite for CEM I, CEM III, CEM IV, and CEM V  
213 cements (Table 1), is completely dissolved into calcium and hydroxide ions at a distance of 2-3 mm  
214 (depending on cement type) from the boundary surface. The depth which corresponds to this total  
215 dissolution, defines the dissolution front of portlandite.

216 The calcium to silicon ratio, drops down to 0 at a depth equivalent to the dissolution front of portlandite  
217 and corresponds to the decalcification front of C-S-H. This total decalcification ( $\text{C/S} = 0$ ) infers that C-  
218 S-H turns into silica gel near the boundary surface.

219 These two dissolutions induce the presence of calcium ions at the common dissolution and  
220 decalcification fronts of portlandite and C-S-H, and these ions react with sulfate ions from sulfuric acid  
221 solution and form a gypsum layer. The thickness of the gypsum layer is 2.0 mm for CEM I and CEM V  
222 cements and 2.4 mm for CEM III and CEM IV cements. The gypsum content at the surface reaches  
223 around 6 mol/L for all the Portland cements. Moreover, ettringite in ordinary or blended Portland

224 cements is considered negligible. The detection of this phase is infrequent in experimental studies [24-  
225 26].

226 For the ordinary and blended Portland cements, porosity is equal to the initial porosity of each  
227 cementitious material until reaching the corresponding depth to the dissolution and decalcification fronts  
228 of portlandite and C-S-H. Indeed, when the two hydrates start to dissolve, new porous space is created  
229 and is partially filled by the precipitation of gypsum, leading to a porosity increase near the boundary  
230 surface. This porosity increase shows that gypsum does not fill the total porosity and its swelling cannot  
231 provoke structural damages.

#### 232 **4.1.2. Profiles of the solid contents for CAC cement**

233 A different behavior is observed for the calcium aluminate cement. The acid attack (Figure 3) leads to  
234 a partial dissolution of the hydrogarnet ( $C_3AH_6$ ). Indeed, the initial hydrogarnet amount is equal to  
235 2 mol/L and decreases to 1.75 mol/L, after 1 year of sulfuric acid attack. The hydrogarnet dissolution is  
236 slower than portlandite dissolution and C-S-H decalcification observed in Portland cements. Gypsum  
237 does not precipitate in this cementitious material, the saturation index being lower than 1 during the  
238 simulation whereas the gibbsite and ettringite precipitate. The ettringite precipitation is due to the  
239 reaction between calcium ions and aluminum ions from the partial dissolution of the hydrogarnet and  
240 sulfate ions from the sulfuric acid solution (the maximum amount reached is  $1.8 \cdot 10^{-1}$  mol/L). This  
241 precipitation tends to clog up the pores of this cementitious material, with the porosity reaching a value  
242 close to zero ( $10^{-10}$  %) at the depth corresponding to the maximum amount of ettringite. When the pH  
243 of the system drops down below 10.7, ettringite starts to dissolve [22] and causes an increase of porosity  
244 which reaches at the boundary surface a value slightly greater than the initial porosity of the CAC (Table  
245 1). The gibbsite forms near the boundary surface with a maximum content reaching  $1.5 \cdot 10^{-1}$  mol/L. This  
246 solid phase fills pores but this precipitation does not compensate the voids created by the dissolution of  
247 ettringite (the molar volume of ettringite is  $710 \text{ cm}^3/\text{mol}$ , whereas that of gibbsite is  $64 \text{ cm}^3/\text{mol}$ ),  
248 resulting in an increase of porosity. As shown in the phase diagram (Figure 2), gypsum is not stable in  
249 presence of hydrogarnet. This is why simulations don't find any gypsum. However, in some

250 experimental studies [35], gypsum can be found in the near surface zones of CAC binders attacked by  
251 sulfuric acid.

252 Damage caused by the ettringite precipitation is not implemented in this study. Experimental studies  
253 [20, 21, 36] have shown some degradations that were explained by the important expansion of ettringite  
254 precipitation (needle like crystals creating locally micro-cracking). In the present study, ettringite fills  
255 the porous space and prevents the sulfuric acid from penetrating into the cementitious material. This  
256 phase has then a protective function.

#### 257 **4.2. Determination of the deterioration depth and of weight loss for different cementitious material** 258 **types**

259 The porosity profiles over depth obtained after one year of acid attack are plotted in Figure 4. The  
260 deterioration depth reached after one year of acid attack and the evolution of this parameter over time  
261 for each cementitious material are respectively proposed in Table 5 and Figure 5.

262 The deterioration depths obtained for CEM I, CEM III, CEM IV, and CEM V cements (Figure 4) are  
263 deeper than that obtained for CAC materials. Specifically, the deterioration depth reached after 1 year  
264 of acid attack for the CAC material is 10 times lower than that for the ordinary or blended Portland  
265 cements (Table 5 and Figure 5). Therefore, the CAC cement paste is clearly the most sustainable cement  
266 in acid conditions. The low deterioration kinetic for CAC materials is observed in many experimental  
267 field and laboratory studies [8, 20, 23, 26, 27, 39, 40]. In the model, this delaying effect is then due to  
268 the better stability of hydrogarnet in acidic conditions than the portlandite and C-S-H and to the ettringite  
269 formation, which clogs up the porosity of the material.

270 Several studies showed that an increase of the porosity causes a decrease of the compressive strength  
271 [37, 38]. The porosity increases from 11 to 22% for CEM I cement, from 14 to 25% for CEM III cement,  
272 from 16 to 26% for CEM IV cement and from 11 to 23% for CEM V cement, whereas the porosity  
273 increases from 10 to 13% for the CAC material. The ordinary or blended Portland cements undergo a

274 comparable decrease of compressive strength and a more important decrease than that of CAC,  
275 highlighted the better resistance of CAC materials to acid attack.

276 Some differences are observed between Portland cements. The deterioration kinetic is quicker for CEM  
277 III and CEM IV cements than for CEM I and CEM V cements (Figure 5). These results are mainly due  
278 to the high porosity of CEM III and CEM IV cements as compared to the porosity of CEM I and CEM  
279 V cements (Table 1). But, these qualitative important differences between these Portland cements need  
280 to be confirmed. Indeed, other hydrates than C-S-H and portlandite for blended Portland cements or  
281 anhydrous phases were not taken into account in the model. Specifically, the phases from the hydration  
282 of blast furnace slag, natural pozzolans, and fly ashes, leading to C-A-S-H and C-S-H with different C/S  
283 ratio and anhydrous phases should be considered.

284 The dissolved calcium contents are determined for each cementitious material after 1 year of sulfuric  
285 acid attack and are presented in Table 6. This parameter is plotted over time (Figure 6) and allows  
286 characterizing cementitious materials deterioration, with data about the loss of matter during the acid  
287 attack.

288 The dissolved calcium content reached after 1 year of sulfuric acid attack for the Portland cements is  
289 more than two times greater than the value for the CAC material (Table 6), highlighting the partial  
290 dissolution of hydrogarnet and the total dissolutions of CH and C-S-H. The evolution of the dissolved  
291 calcium content is linear with  $\sqrt{t}$  for CEM I, CEM III, CEM IV, and CEM V cements. For CAC cement,  
292 this parameter is almost linear with time. But, this evolution is considered as linear with  $\sqrt{t}$  (the  
293 correlation coefficient is equal to 0.92), in order to compare the cementitious materials.

#### 294 **4.3. Long-term prediction**

295 The deterioration depths obtained are only calculated over 1 year of sulfuric acid attack. Yuan et al. [15]  
296 considered the evolution of the deterioration depth over time as a linear function of the square root of  
297 time, i.e.  $K\sqrt{t}$ . The proportionality with the square root of time is characteristic of a diffusion process.

298 The values of K for all cementitious materials are shown in Table 7 and are considered equal to  
299 deterioration rates.

300 The deterioration rate obtained for the CAC material is 10 times lower than the deterioration rates for  
301 the Portland cements (Table 7). The field tests from literature [8, 38, 39] showed a corrosion rate 4 times  
302 lower for the CAC material in regard to CEM I cement. Consequently, this model overestimates the  
303 better resistance of CAC materials, but it qualitatively consistent with observations. Moreover, the aim  
304 of these simulations is to give chemical-based understanding of the better resistance of CAC cement  
305 already observed with *in-situ* or laboratory tests. The partial dissolution of hydrogarnet shows that this  
306 type of cement is constituted of hydrate resistant to acid conditions.

## 307 5. Conclusion

308 In this study, the effect of the cementitious material types on the deterioration obtained during 1 year of  
309 sulfuric acid attack is evaluated with a chemical-reactive transport model.

310 The main results of the modeling highlight that the deterioration kinetic of the CAC materials is slower  
311 than that of other cements (CEM I, CEM III, CEM IV and CEM V), as observed in several field tests.  
312 This better resistance is mainly explained by the better thermodynamic stability in acidic conditions of  
313 hydrogarnet compared to portlandite and C-S-H and to the ettringite precipitation which prevents the  
314 penetration of sulfuric acid with a pore-blocking effect. But, this better resistance needs to be qualified  
315 due to the ettringite precipitation, difficult to reconcile with some experimental studies.

316 The main perspectives for this sulfuric acid deterioration model are first, the implementation of a damage  
317 model for the gypsum swelling and the ettringite precipitation for all the cementitious materials studied.

318 The second point to improve obviously concerns the consideration of the microorganisms which produce  
319 sulfuric acid in sewer networks. Indeed, the factors controlling bio receptivity of cementitious materials,  
320 which ultimately steers the acid production, are essential for modelling. Finally, the third point is the  
321 inclusion of additional phases for blended Portland cements (blast furnace slag, pozzolans, and fly ashes)  
322 in order to better represent these kinds of cements.

323 **Acknowledgment**

324 This study was carried out in the frame of the FUI Duranet project and funded by BpiFrance (contract  
325 F1409022M).

326

327

328

329 **References**

330 [1] Brongers M., Koch G., Thompson N., Corrosion costs and preventive strategies in the United States,  
331 Report FHWA-RD-01-156, 2001, Federal Highway Administration, Washington, DC.

332 [2] Zhang L., De Schryver P., De Gusseme B., De Muyneck W., Boon N. and Verstraete W., Chemical  
333 and biological technologies for hydrogen sulfide emission control in sewer systems: a review, *Water*  
334 *Research* 42 (2008): 1-12.

335 [3] Boon A.G., Specificity in sewers: causes, consequences and containments, *Water Science*  
336 *Technology* 31 (1995): 237-253.

337 [4] Joseph A.P., Keller J., Bustamante H. and Bond P.L., Surface neutralization and H<sub>2</sub>S oxidation at  
338 early stages of sewer corrosion: Influence of temperature, relative humidity and H<sub>2</sub>S concentration,  
339 *Water Research* 46 (2012): 4235-45.

340 [5] Islander R.L., Deviny J.S., Mansfeld F., Postyn A. and Shih H., Microbial ecology of crown  
341 corrosion in sewers, *Journal of Environmental Engineering* 117 (1991): 761-770.

342 [6] Okabe S., Odagiri M., Ito, T. and Satoh H., Succession of sulfur-oxidizing bacteria in the microbial  
343 community on corroding concrete in sewer systems, *Applied and Environmental Microbiology* 73  
344 (2007): 971-80.

345 [7] Davis J.L., Nica D., Shields K. and Roberts D.J., Analysis of concrete from corroded sewer pipe,

Grandclerc A., Dangla P., Gueguen-Minerbe M., Chaussadent T., *Modelling of the sulphuric acid attack on different types of cementitious materials, Cement and Concrete Research* 105 (2018) 126–133

346 *International Biodeterioration & Biodegradation* 42 (1998): 75 - 84.

347 [8] Alexander M. G. and Fourie C., Performance of sewer pipe concrete mixtures with Portland and  
348 calcium aluminate cements subject to mineral and biogenic acid attack, *Materials and Structures* 44  
349 (2010): 313-30.

350 [9] Pavlík V., Corrosion of hardened cement paste by acetic and nitric acids part I: Calculation of  
351 corrosion depth, *Cement and Concrete Research* 24 (1994): 551 -62.

352 [10] Nielsen A.H., Hvitved-Jacobsen T. and Vollertsen J., Kinetics and stoichiometry of sulfide  
353 oxidation by sewer biofilms, *Water Research* 39 (2005): 4119-25.

354 [11] Jensen H.S., Nielsen A.H., Hvitved-Jacobsen T. and Vollertsen J., Modeling of hydrogen sulfide  
355 oxidation in concrete corrosion products from sewer pipes, *Water Environment Research* 81 (2009):  
356 365-73.

357 [12] Jahani F., Deviny J., Mansfeld F., Rosen I.G., Sun Z. and Wang C., Investigations of sulfuric acid  
358 corrosion of concrete. II: electrochemical and visual observations, *Journal of environmental engineering*  
359 127 (2001): 580–584.

360 [13] Van der Lee G., De Windt L., Lagneau V. and Goblet P., Module-oriented modeling of reactive  
361 transport with HYTEC, *Computers & Geosciences* 29 (2003): 265-75.

362 [14] De Windt L. and Devillers P., Modeling the degradation of Portland cement pastes by biogenic  
363 organic acids, *Cement and Concrete Research* 40 (2010): 1165-74.

364 [15] Yuan H., Dangla P., Chatellier P. and Chaussadent T., Degradation modelling of concrete submitted  
365 to sulfuric acid attack, *Cement and Concrete Research* 53 (2013): 267-77.

366 [16] Chalupecký, V., Fatima T., Kruschwitz J. and Muntean A., CASA-Report 12-01 January 2012.

367 [17] Yuan H., Dangla P., Chatellier P. and Chaussadent T., Degradation modeling of concrete submitted

Grandclerc A., Dangla P., Gueguen-Minerbe M., Chaussadent T., *Modelling of the sulphuric acid attack on different types of cementitious materials, Cement and Concrete Research* 105 (2018) 126–133

368 to biogenic acid attack, *Cement and Concrete Research* 70 (2015): 29–38.

369 [18] Bassuoni M.T. and Nehdi M.L., Resistance of self-consolidating concrete to sulfuric acid attack  
370 with consecutive pH reduction, *Cement and Concrete Research* 37 (2007): 1070-84.

371 [19] Kawai K., Sako A., Ikuta T. and Ishida T., Deterioration of cement hydrates containing mineral  
372 admixtures due to sulfuric acid attack, *In IIDBMC International Conference on Durability of Building*  
373 *Materials and Components*, Istanbul, Turkey, 2008.

374 [20] Herisson J., Van Hullebusch E.D., Moletta-Denat M., Taquet P. and Chaussadent T., Toward an  
375 accelerated biodeterioration test to understand the behavior of Portland and Calcium Aluminate  
376 cementitious materials in sewer networks, *International Biodeterioration & Biodegradation* 84 (2013):  
377 236-43.

378 [21] Jiang G., Wightman E., Bogdan C. D., Yuan Z., Bond P.L. and Keller J., The role of iron in sulfide  
379 induced corrosion of sewer concrete, *Water Research* 49 (2014): 166-74.

380 [22] Gabrisova A., Havlica J. and Sahu S., Stability of calcium sulphoaluminate hydrates in water  
381 solutions with various pH values, *Cement and Concrete Research* 21 (1991): 1023–1027.

382 [23] Herisson J., Guéguen-Minerbe M., Van Hullebusch E.D. and Chaussadent T., Behaviour of  
383 different cementitious material formulations in sewer networks, *Water Science & Technology* 69 (2014):  
384 1502.

385 [24] Schmidt M., Hormann K. and Hofmann F., Stability of concrete against biogenic sulfuric acid  
386 corrosion, a new method for determination, *In Proceedings of the 10th international congress on the*  
387 *chemistry of cement*, Gothenburg, 1997.

388 [25] Ehrich S., Helard L., Letourneux R., Willocq J. and Bock E., Biogenic and chemical sulfuric acid  
389 corrosion of mortars, *Journal of materials in civil engineering* 11 (1999): 340–344.

390 [26] Miokono, D.H.E, Biodétérioration de mortiers avec une succession de bactéries sulfo-oxydantes

Grandclerc A., Dangla P., Gueguen-Minerbe M., Chaussadent T., *Modelling of the sulphuric acid attack on different types of cementitious materials, Cement and Concrete Research* 105 (2018) 126–133

- 391 neutrophiles et acidophiles, PhD at the University of Lille 1, 2013, 365 pages.
- 392 [27] Peyre Lavigne M., Bertron A., Auer L., Hernandez-Raquet G., Foussard J.N., Escadeillas G., Cockx  
393 A. and Paul E., An innovative approach to reproduce the biodeterioration of industrial cementitious  
394 products in a sewer environment. Part I: Test design, *Cement and Concrete Research* 73 (2015): 246-  
395 56.
- 396 [28] NF P18-459, “Concrete – Hardened concrete test – Porosity and density tests”, French standard,  
397 2010.
- 398 [29] Nilforushan M.R and Talebian N., The hydration products of a refractory calcium aluminate cement  
399 at intermediate temperatures, *Iran. J. Chem. Eng* 26 (2007).
- 400 [30] Lamberet S., Guinot D., Lempereur E., Talley J. and Alt C., Fields investigations of high  
401 performance calcium aluminate mortar for wastewater applications, *Calcium aluminate cements,*  
402 *proceeding of the centenary conference, Avignon, IHS BRE Press, 2008.*
- 403 [31] Damidot D., Lothenbach B., Herfort D. and Glasser F.P., Thermodynamic and cement science,  
404 *Cement and Concrete Research* 41 (2011): 679-695.
- 405 [32] Dangla P., Thiery M. and Morandea A., Thermodynamic of incongruent solubility of C-S-H,  
406 *Advances in Cement Research* (2015) (*online version*).
- 407 [33] Dangla P., Bil-2.4, A modeling platform based on finite volume/element method, doi:  
408 10.5281/zenodo.1039729, 2017.
- 409 [34] Bazant Z.P. and Najjar L.J., Nonlinear water diffusion in nonsaturated concrete, *Materials and*  
410 *structures* 5(1972): 3-20.
- 411 [35] Proceedings of the RILEM TC-211-PAE, Performance of cement-based materials in aggressive  
412 aqueous environments, Springer (2013), ISBN 978-94-007-5419-3.
- 413 [36] Mori T., Nonaka M., Tazaki K., Koga M., Hikosaka Y. and Noda S., Interactions of nutrients,

Grandclerc A., Dangla P., Gueguen-Minerbe M., Chaussadent T., *Modelling of the sulphuric acid attack on different types of cementitious materials, Cement and Concrete Research* 105 (2018) 126–133

414 moisture and pH on microbial corrosion of concrete sewer pipes, *Water Research* 26 (1991): 29–37.

415 [37] Lee H.S., Ismail M.A., Woo Y.J., Min T.B. and Choi H.C., Fundamental study on the development  
416 of structural lightweight concrete by using normal coarse aggregate and foaming agent, *Materials* 7  
417 (2014): 4536–4554.

418 [38] Zhao H., Xiao Q., Huang D. and Zhang S., Influence of pore structure on compressive strength of  
419 cement mortar, *Scientific World Journal*, Article ID 247058, 2014.

420 [39] Goyns A., Calcium aluminate cement linings for cost-effective sewers, *In International conference*  
421 *on calcium aluminate cements*, 6317–6319, 2001.

422 [40] Alexander M. G., Goyns A. and Fourie C.W., Experiences with a full-scale experimental sewer  
423 made with CAC and other cementitious binders in Virginia, South Africa, In Proceedings, *calcium*  
424 *aluminate cements, the centenary conference*. IHS BRE Press, Bracknell, 279–292, 2008.

425

Cement	$n_{CH}$ (mol/L)	$n_{CSH}$ (mol/L)	$n_{C_3AH_6}$ (mol/L)	$n_{AH_3}$ (mol/L)	Porosity (%)
CEM I	1.84	2.45	-	-	11
CEM III	1.18	2.83	-	-	18
CEM IV	0.75	3.10	-	-	16
CEM V	1.19	2.84			11
CAC	-	-	2	0	10

Table 1: Hydrate amounts and porosity for cement pastes based on CEM I, CEM III, CEM IV, CEM V cements, and CAC.

426  
427

428

Solid phases	Dissolution reactions	Thermodynamic constant (K)
Portlandite (CH)	<b>Reaction involving calcium compounds</b> $Ca(OH)_2 \rightleftharpoons Ca^{2+} + 2OH^-$	$8.90 \cdot 10^{-6}$
Gibbsite (AH <sub>3</sub> )	<b>Reaction involving aluminum compounds</b> $Al(OH)_3 \rightleftharpoons Al^{3+} + 6OH^-$	$1.0 \cdot 10^{-68}$
Gypsum (C $\bar{S}$ H <sub>2</sub> )	<b>Reaction involving calcium-sulfur compounds</b> $CaSO_4 \cdot 2H_2O \rightleftharpoons Ca^{2+} + SO_4^{2-} + 2H_2O$	$3.72 \cdot 10^{-5}$
AFm (C <sub>4</sub> A $\bar{S}$ H <sub>12</sub> )	<b>Reactions involving calcium-aluminum-sulfur compounds</b> $3CaO \cdot Al_2O_3 \cdot CaSO_4 \cdot 12H_2O \rightleftharpoons 4Ca^{2+} + 2Al(OH)_4^- + 4OH^- + SO_4^{2-} + 6H_2O$	$3.71 \cdot 10^{-30}$
Ettringite (C <sub>3</sub> A $\bar{S}$ <sub>3</sub> H <sub>32</sub> )	$3CaO \cdot Al_2O_3 \cdot 3CaSO_4 \cdot 32H_2O \rightleftharpoons 6Ca^{2+} + 2Al(OH)_4^- + 3SO_4^{2-} + 4OH^- + 26H_2O$	$2.80 \cdot 10^{-45}$
Hydrogarnet (C <sub>3</sub> AH <sub>6</sub> )	<b>Reactions involving calcium-aluminum compounds</b> $3CaO \cdot Al_2O_3 \cdot 6H_2O \rightleftharpoons 3Ca^{2+} + 2Al(OH)_4^- + 4OH^-$	$3.2 \cdot 10^{-21}$
C <sub>2</sub> AH <sub>8</sub>	$2CaO \cdot Al_2O_3 \cdot 8H_2O \rightleftharpoons 2Al(OH)_4^- + 2Ca^{2+} + 3H_2O + 2OH^-$	$2.8 \cdot 10^{-14}$
CAH <sub>10</sub>	$CaO \cdot Al_2O_3 \cdot 10H_2O \rightleftharpoons 2Al(OH)_4^- + Ca^{2+} + 6H_2O$	$2.5 \cdot 10^{-8}$
C-S-H	<b>Reaction involving calcium-silicon compounds</b> $C_xS_yH_z \rightleftharpoons xCa^{2+} + 2xOH^- + ySiO_2^0 + (z-x) H_2O$	See [15]
Silica gel (SH)	<b>Reaction involving silicon compounds</b> $SH_u \rightleftharpoons SiO_2^0 + uH_2O$	$1.74 \cdot 10^{-3}$

Table 2: Heterogeneous reactions taking place in the CaO-Al<sub>2</sub>O<sub>3</sub>-SiO<sub>2</sub>-SO<sub>3</sub>-H<sub>2</sub>O system

429

430

Dissociation reactions	Thermodynamic constant (K)
<b>Reaction involving calcium compounds</b> $\text{Ca(OH)}_2^0 \rightleftharpoons \text{Ca}^{2+} + 2\text{OH}^-$ $\text{Ca(OH)}^+ \rightleftharpoons \text{Ca}^{2+} + \text{OH}^-$	1 $1.66 \cdot 10^1$
<b>Reactions involving silicon compounds</b> $\text{SiO}_2^0 + 2\text{H}_2\text{O} \rightleftharpoons \text{H}_4\text{SiO}_4^0$ $\text{H}_4\text{SiO}_4^0 \rightleftharpoons \text{H}_3\text{SiO}_4^- + \text{H}^+$ $\text{H}_3\text{SiO}_4^- \rightleftharpoons \text{H}_2\text{SiO}_4^{2-} + \text{H}^+$ $\text{H}_2\text{SiO}_4^{2-} \rightleftharpoons \text{HSiO}_4^{3-} + \text{H}^+$	$1.94 \cdot 10^{-3}$ $1.55 \cdot 10^{-10}$ $4.68 \cdot 10^{-14}$ $1.0 \cdot 10^{-15}$
<b>Reaction involving sodium compounds</b> $\text{NaOH}^0 \rightleftharpoons \text{Na}^+ + \text{OH}^-$	1.5
<b>Reaction involving potassium compounds</b> $\text{KOH}^0 \rightleftharpoons \text{K}^+ + \text{OH}^-$	2.9
<b>Reactions involving sulfur compounds</b> $\text{H}_2\text{SO}_4^0 \rightleftharpoons \text{HSO}_4^- + \text{H}^+$ $\text{HSO}_4^- \rightleftharpoons \text{SO}_4^{2-} + \text{H}^+$	$1.0 \cdot 10^6$ $1.0 \cdot 10^{-2}$
<b>Reaction involving aluminum compounds</b> $\text{Al(OH)}_4^- \rightleftharpoons \text{Al}^{3+} + 4\text{OH}^-$	$6.2 \cdot 10^{-34}$
<b>Reactions involving calcium-silicon compounds</b> $\text{CaH}_2\text{SiO}_4^0 \rightleftharpoons \text{Ca}^{2+} + \text{H}_2\text{SiO}_4^{2-}$ $\text{CaH}_3\text{SiO}_4^+ \rightleftharpoons \text{Ca}^{2+} + \text{H}_3\text{SiO}_4^-$	$3.89 \cdot 10^4$ $1.56 \cdot 10^1$
<b>Reaction involving calcium-sulfur compounds</b> $\text{Ca}^{2+} + \text{SO}_4^{2-} \rightleftharpoons \text{CaSO}_4^0$ $\text{Ca}^{2+} + \text{HSO}_4^- \rightleftharpoons \text{CaHSO}_4^+$	$1.4 \cdot 10^{-3}$ $1.3 \cdot 10^1$

431 **Table 3: Homogeneous aqueous reactions taking place in CaO-Al<sub>2</sub>O<sub>3</sub>-SiO<sub>2</sub>-SO<sub>3</sub>-Na<sub>2</sub>O-K<sub>2</sub>O-H<sub>2</sub>O**  
 432 **system**

433

Solid phases	R <sub>A</sub> (mol/L/s) for Portland cements	R <sub>A</sub> (mol/L/s) for CAC cement
C $\bar{\text{S}}$ H <sub>2</sub> (gypsum)	$1 \cdot 10^{-4}$	$1 \cdot 10^{-7}$
AFt	$1 \cdot 10^{-11}$	$1 \cdot 10^{-7}$
AFm	$1 \cdot 10^{-11}$	$1 \cdot 10^{-11}$
C <sub>3</sub> AH <sub>6</sub>	-	$1 \cdot 10^{-8}$

434 **Table 4: Kinetic factors of the solid phases for the CaO-Al<sub>2</sub>O<sub>3</sub>-SO<sub>3</sub>-H<sub>2</sub>O system.**

435

Cement pastes	Deterioration depths (mm)
CEM I	2.0
CEM III	2.4
CEM IV	2.8
CEM V	2.2
CAC	0.2

436 **Table 5: Deterioration depths obtained for CEM I, CEM III, CEM IV, CEM V cements and**  
 437 **CAC after 1 year of acid attack at  $10^{-1}$  mol/L.**

Materials	Dissolved calcium amount (g/L)	Weight loss (%)
CEM I	90	37.5
CEM III	80	33.3
CEM IV	80	33.3
CEM V	80	33.3
CAC	35	14.6

438 **Table 6: Dissolved calcium contents obtained for CEM I, CEM III, CEM IV, CEM V cements,**  
 439 **and CAC after 1 year of sulfuric acid attack at  $10^{-1}$  mol/L.**

Materials	Corrosion rates (mm/year <sup>0.5</sup> )
CEM I	0.10
CEM III	0.11
CEM IV	0.14
CEM V	0.10
CAC	0.01

440 **Table 7: Corrosion rates obtained for CEM I, CEM III, CEM IV, CEM V cements, and CAC.**

441

442 **Figure captions**

443 **Figure 1:** Concrete sewer and biodeterioration mechanisms. SRB are sulfate-reducing bacteria and SOB  
 444 are sulfur-oxidizing bacteria.

445 **Figure 2:** Phase Diagram for the system CaO-Al<sub>2</sub>O<sub>3</sub>-SO<sub>3</sub>-H<sub>2</sub>O. This diagram is constituted of the  
 446 simultaneous evolutions of the saturation indexes of AH<sub>3</sub> ( $\beta_{AH3}$ ) and CH ( $\beta_{CH}$ ) with the H<sub>2</sub>SO<sub>4</sub>  
 447 concentration ( $a_{H2SO4}$ ) in logarithmic scale.

448 **Figure 3:** Profiles of the solid phases (CH, C<sub>3</sub>AH<sub>6</sub>, AFt, AH<sub>3</sub>, and C $\bar{S}$ H<sub>2</sub> (gypsum)), of the calcium to  
 449 silicon ratio and of the porosity, for cementitious materials based on CEM I, CEM III, CEM IV, CEM V  
 450 cements, and CAC, after 1 year of acid attack.

451 **Figure 4:** Evolution of the porosity over depth for the cementitious materials based on CEM I, CEM III,  
 452 CEM IV, CEM V cements, and CAC during 1 year of sulfuric acid attack at  $10^{-1}$  mol/L. The black circles  
 453 represent the point where porosity becomes superior to the initial porosity of each cementitious material.

454 **Figure 5:** Evolution of the deterioration depth for cementitious materials based on CEM I, CEM III,  
 455 CEM IV, CEM V cements, and CAC over time, during 1 year of acid attack at  $10^{-1}$  mol/L.

456 **Figure 6:** Dissolved calcium contents over time for cementitious materials based on CEM I, CEM III,  
 457 CEM IV, CEM V cements, and CAC during 1 year of sulfuric acid attack at  $10^{-1}$  mol/L.

458

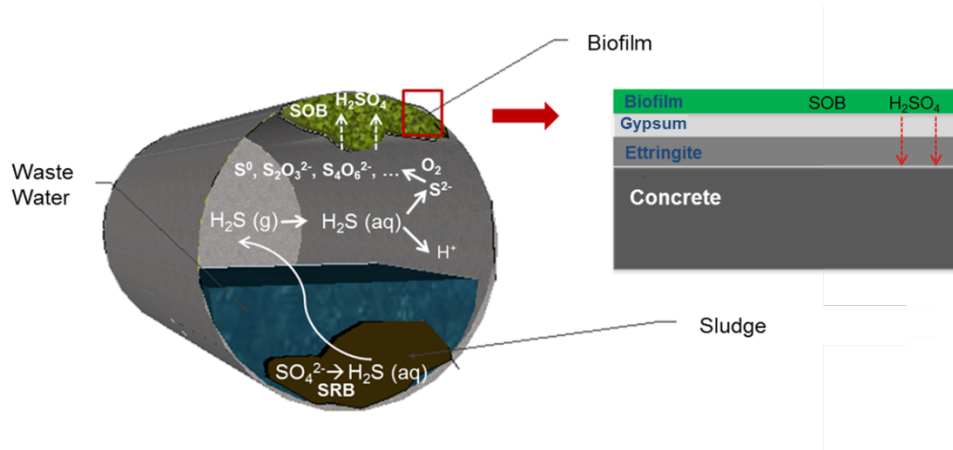
459

460

461

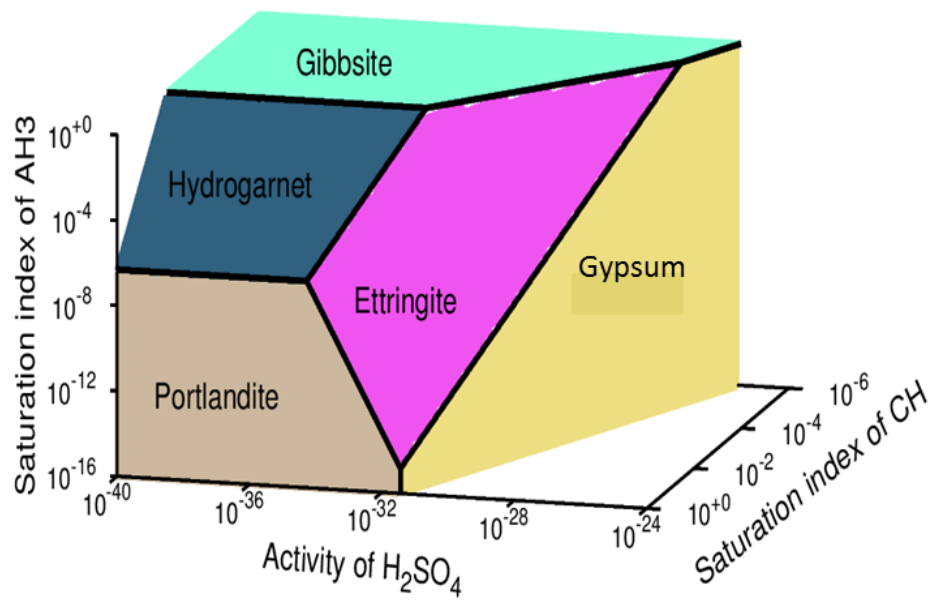
462

463 **FIGURE 1.**



464

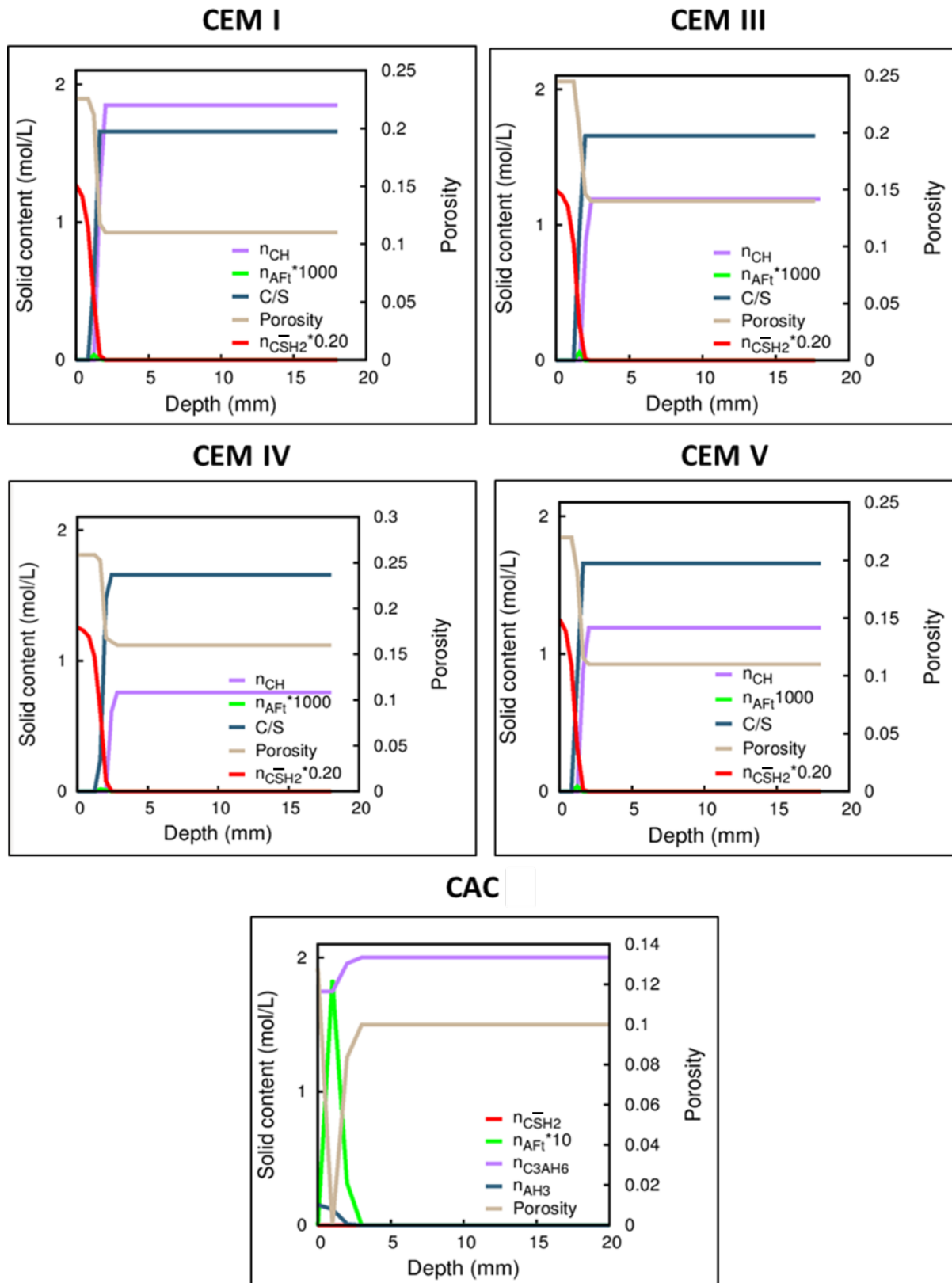
465 **FIGURE 2.**



466

467

468 **FIGURE 3.**

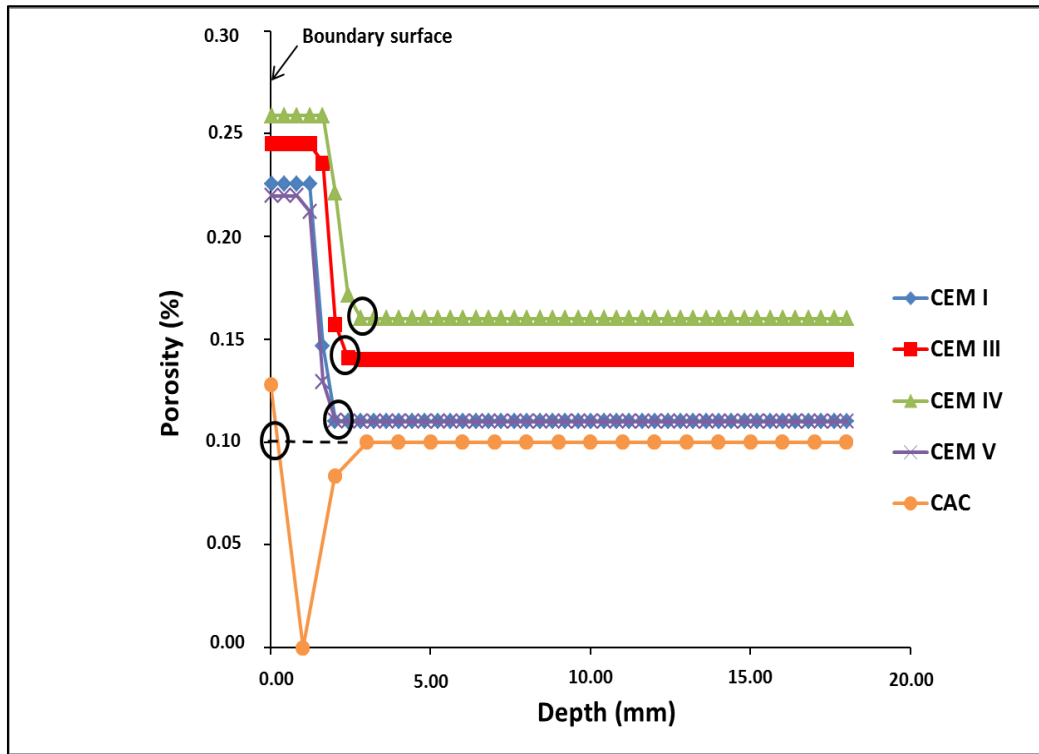


469

470

471

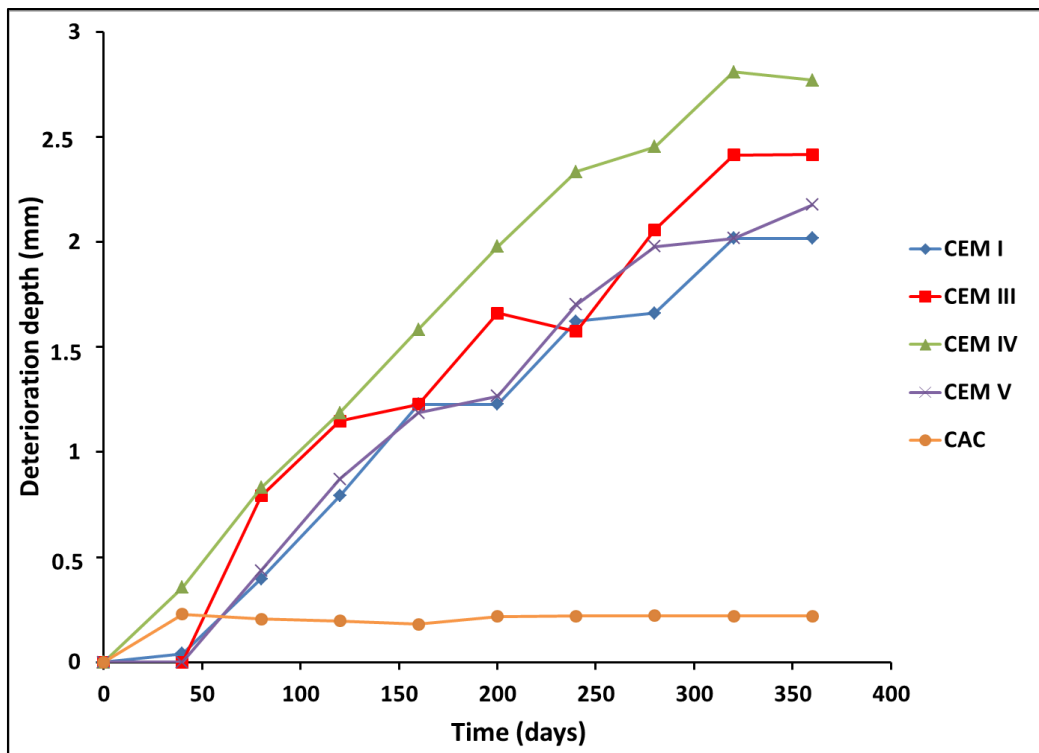
472 **FIGURE 4.**



473

474

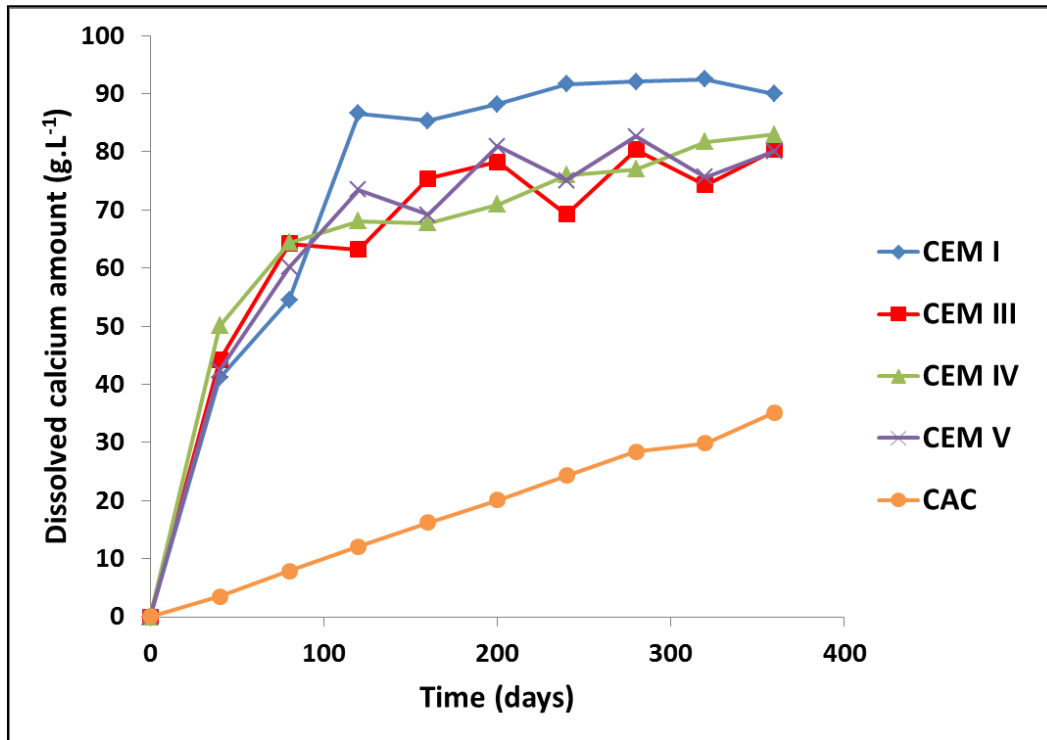
475 **FIGURE 5.**



476

477

478 **FIGURE 6.**



479

480

481

482

483

484

485

486

487

488

489

490

491

492